Korean J. Chem. Eng., 35(7), 1450-1461 (2018)
DOI: 10.1007/s11814-018-0052-6

pISSN: 0256-1115
eISSN: 1975-7220

Physical and adsorptive characterizations of immobilized polyaniline for the removal of methyl orange dye

Noor Nazihah Bahrudin*,†, Mohd Asri Nawi*, and Wan Izhan Nawawi Wan Ismail,*****

*School of Chemical Sciences, Universiti Sains Malaysia, 11800 Penang, Malaysia
**Photocatalysis Laboratory, FSG, Universiti Teknologi MARA, 02600 Arau, Perlis, Malaysia
***Department of Chemistry, University of York, Heslington, York, YO10 5DD, United Kingdom
(*Received 21 December 2017 • accepted 21 March 2018*)

Abstract−Synthesized polyaniline (PANI) powder mixed with ENR-PVC polymer blend adhesive was immobilized on glass plates for the adsorption of methyl orange (MO) dye. The immobilized PANI composite was made up of plasticized PANI aggregates and was in a doped state. The incorporation of ENR-PVC blend in PANI slightly reduced the surface area from 9.2 to 8.5 $m^2 g^{-1}$, and its presence was confirmed through FTIR. The adsorption process was highly dependent on the aeration rate, and the pH of MO solution in which 40 mL min^{-1} and ambient pH (6.5) was selected as the working conditions. The process of MO uptake onto the immobilized PANI obeyed the pseudo-second-order kinetic model, while intra-particle diffusion was found to dominate the adsorption process. The q_m of the immobilized PANI was 77.3 mg g^{-1} for MO uptake and obeyed the Freundlich isotherm model. The thermodynamic study revealed that the adsorption process of immobilized PANI was spontaneous and unfavorable at high temperature. The immobilized PANI was found to be comparable with other PANI based adsorbents in term of cost, recyclability and adsorption efficiency.

Keywords: Immobilized Polyaniline, Adsorption Isotherm, Kinetic Modeling, Methyl Orange, Thermodynamic

INTRODUCTION

Water pollutants, such as dyes [1,2], heavy metals [3], herbicides [4,5] and pharmaceutical wastes [6,7], have been polluting water sources and mainstreams globally. Dyes, for instance, are produced annually by 450,000 tons in which 40,000 tons of the overall amount end up as effluent [8]. Due to the toxicity of the pollutants, especially dyes, many treatment techniques have been developed to remove them from the waterways, including electrocoagulation [9], magnetic separation [10], photocatalytic oxidation [11,12] and ion exchange [13]. Despite so, the adsorption process still fascinates the global researchers due to its simplicity, high removal efficiency and the availability of a wide range of adsorbents such as bagasse fly ash [14], activated carbon [15], chitosan [16], clay [17], iron nano [18,19], beach sand [20] and newspaper waste [21].

Amongst the preferred adsorbents in wastewater treatment is polyaniline (PANI), which is a conjugated polymer. PANI has been used as an adsorbent for the removal of humic acid [22], dyestuffs [23,24] and heavy metals [25,26]. Structurally, PANI is a phenylene-based polymer having -NH- group on either side of the phenylene ring. It exists in three oxidation states, which are leucoemeraldine base (fully reduced), emeraldine base (partially oxidized) and pernigraniline base (fully oxidized) [27]. The attractive applications of PANI are due to the redox reaction that takes place on this -NH-group in which various forms of PANI can be obtained from the number of imine and amine segments in the PANI chains [28]. In addition, the ease of synthesis, high stability in the environment and high electrical conductivity make PANI as one of the future valuable materials [22]. PANI can be also synthesized via various methods, such as seeding [29], metathesis [30], self-assembling [31], electrochemical [32,33] and sonochemical [34]. Recently, the synthesis of PANI via a facile route of chemical polymerization in an acidic medium has received attention, as it can avoid the unnecessary formation of precipitation and use of sophisticated instruments [35]. Moreover, PANI powder produced by this method is in a bulk quantity, more pure, uniform, porous and can be produced at room temperature [35-38].

The conventional suspended mode is frequently utilized for the application of PANI powder, which requires tedious post-treatment and difficult recovery steps consuming time and money [3,39]. In this case, immobilization of PANI powder on the supporting materials seems to be the best solution, while the blending of two polymer adhesives is suitable for binding the PANI powder on the support materials. For this study, the selection of epoxidized natural rubber-poly (vinyl) chloride blend (ENR-PVC) is based on the successful immobilization of TiO_2 powder on the glass supports [11,40]. It has been reported that PVC has an excellent chemical and physical properties, low cost, robust and high stiffness, while ENR is a good elastomer due to its flexibility, hydrophilicity and high shearing [41]. The interaction of ENR and PVC is induced by the highly polar epoxide groups within the ENR, whereby ENR offers elasticity and gel properties while PVC provides mechanical strength to the polymer blend [41,42]. Their individual properties eventually improve

†To whom correspondence should be addressed.
E-mail: nazihah.noor@yahoo.com

the properties of the polymer blend in terms of mechanical, environmental and rheological [12]. This polymer blend is also miscible at all compositional ranges [43]. Hence, it is very attractive to use this ENR-PVC polymer adhesive for the purpose of immobilization of PANI powder as there is no published work on PANI-ENR-PVC composite, at the time this article is written.

This study came out with the aim to show that the synthesized PANI powder can be immobilized on the solid supports using ENR-PVC adhesive and has good adsorption efficiency towards methyl orange (MO) in aqueous solution. The effect of selected parameters that would influence the adsorption process by immobilized PANI was extensively studied. The kinetic, isotherm and thermodynamic data were evaluated accordingly based on the respective adsorption modeling to better understand the MO adsorption mechanism, and the results were compared against PANI in suspended mode. In addition, the reusability of the immobilized PANI for three consecutive cycles without effective desorption process was also presented.

EXPERIMENTAL

1. Materials and Reagents

Aniline ($C_6H_5NH_2$, ≥99.5%) and ammonium persulfate (APS, ≥98%) were purchased from Sigma Aldrich. Concentrated sulfuric acid (H_2SO_4, 95-97%) from Merck was diluted to 0.5 M with ultra-pure water (18.2 MΩcm^{-1}). Epoxidized natural rubber (ENR, 50% epoxidation) and polyvinyl chloride (PVC) powder were supplied from Guthrie Group Sdn. Bhd. and Petrochemical (M) Sdn Bhd, respectively. ENR was refluxed in 250 mL toluene at 88-90 °C until all solids dissolved in the viscosity range of 11-13% (w/v). Toluene (C_7H_8) and dichloromethane (CH_2Cl_2) for ENR and PVC dissolution, respectively, were obtained from Q Rec. Methyl orange (Fig. 1), (MO, color index no: C.I 13025, molecular weight: 327.33 g mol^{-1}, molecular formula: $C_{14}H_{14}N_3NaO_3S$) was a product from BDH Ltd. Hydrochloric acid (HCl, 37.0%) and sodium hydroxide (NaOH) pellets for the pH adjustment were purchased from Q Rec and Merck, respectively. All chemicals were analytical grade and used as received without purification.

2. Synthesis of PANI Powder

6 mL of aniline was pipetted into a beaker containing 100 mL of 0.5 M H_2SO_4 and the mixture was stirred for 30 min at room temperature. In a different beaker, 15 g of APS was dissolved in 100 mL of 0.5 M H_2SO_4 and was added in dropwise into the aniline solution under constant stirring. The dark green solution emerged after 5 min, indicating polymerization had begun and the solution was left being stirred for another 7 h. Then, the precipitate PANI solution was dried in an oven at 60 °C. To remove excessive acid, the dried PANI was washed with enough distilled water by centrifugation until the filtrate water increased to pH 3 and was rinsed with methanol and lastly with acetone. The rinsed PANI was dried completely in the oven at 60 °C. PANI powder was obtained after grinding and sieving the dried PANI with a 150 μm mesh siever. This preparation yielded about 5±1 g of dark green PANI powder.

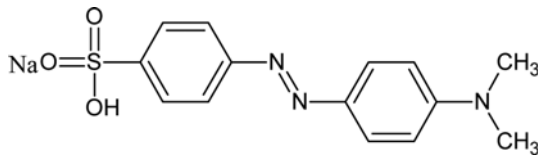

Fig. 1. Molecular structure of methyl orange (MO).

3. Preparation of Immobilized PANI

0.8 g of PVC powder was dissolved in 35 mL of dichloromethane by sonication while 4 g of ENR solution was dissolved in 65 mL of toluene, separately following the published method by Nawi and Zain [40]. Both solutions were mixed homogeneously in a bottle before adding 5 g of the synthesized PANI powder. The bottle containing PANI powder and ENR-PVC solution was sonicated for 3 h and then ground using a ball-mill grinder for 2 h at 40 rpm. Plates with 4.7 cm×7.0 cm×0.2 cm of dimension were coated with the PANI-ENR-PVC formulation by a dip-coating method for desired loadings as determined by the difference in weight before and after dip-coating [40]. The coated plates, later known as immobilized PANI, were then neutralized (pH 7) by 0.1 M NaOH solution in distilled water to eliminate residual acid and were dried completely before use.

4. Physical Characterization

The surface morphology of PANI powder and immobilized PANI (PANI-ENR-PVC composite) was examined under a scanning electron microscope, SEM (LEO Supra 50 VP Field Emission model) equipped with the energy dispersive X-ray, EDX (X'Pert PRO). The BET surface area and porosity of the samples were analyzed using a physisorption analyzer (ASAP 2010, Micromeritics) while the Fourier transform infrared (FTIR) (Series 2000, Perkin Elmer) was used to investigate the corresponding functional groups in the range of 400-4,000 cm^{-1} and resolution scans of 4 cm^{-1}. The optical property of PANI powder and immobilized PANI was observed via a UV-visible diffuse reflectance spectroscopy, UV-vis DRS (Lambda 35, Perkin Elmer) using a magnesium oxide (MgO) disc as the blank in the range of 350-800 nm. Meanwhile, the X-ray diffraction (XRD) analysis was done on a single-crystal Supernova with dual Mo and Cu sources and a Bruker D8 powder diffractometer equipped with a Cu source.

5. Adsorption Experiment and Data Evaluation

20 mL of MO solution each, with respective concentration, was aerated in a glass cell containing either an immobilized PANI or PANI powder as shown in Supplementary Fig. 1. Briefly, the adsorption process was initialized when aeration was supplied via a Pasteur pipette attached to an aquarium air pump by PVC tubing, whereby the air flow rate was controlled using a Gilmont flow meter. Several experimental variables were chosen, such as aeration flow rate (0-100 mL min^{-1}), initial pH of MO solutions (3-11), and initial MO concentrations (20-60 mg L^{-1}), while the loading of immobilized PANI and PANI powder was fixed at 0.63 mg cm^{-1} and 20 mg, respectively. pH of MO solution was adjusted using either 0.1 M HCl or 0.1 M NaOH and was measured using a pH meter (pH 211, HANNA Instruments). For the thermodynamic study, the temperature of the water bath was adjusted to 30-60 °C. A reusability study of immobilized PANI was done for three cycles, whereby at the beginning of each reuse cycle, ultra-pure water was used to clean up the film surface for 30 min and a new solution of 20 mg L^{-1} MO was added into the reactor cell. The absorbance

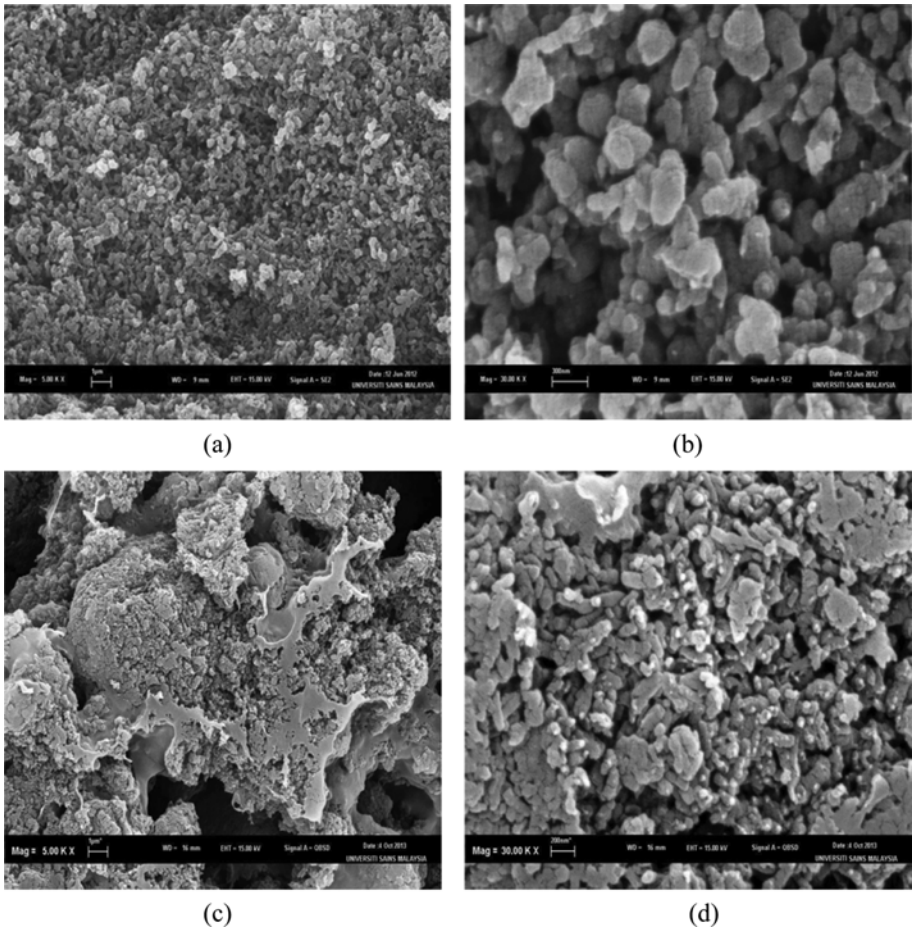

Fig. 2. SEM images of PANI powder under; (a) 5,000 x, (b) 30,000 x of magnifications, and immobilized PANI under; (c) 5,000 x, (d) 30,000 x of magnifications.

change in MO dye solution was measured at 464 nm using a direct reading spectrophotometer (DR2100, HACH).

The amount of dye adsorbed, q_e, and the percentage of MO removed (R) were calculated as follows:

$$q_e\ (\text{mg g}^{-1}) = \frac{(C_o - C_e)V}{W} \quad (1)$$

$$R\ (\%) = \frac{(C_o - C_e)}{C_o} \times 100 \quad (2)$$

where, C_o is the initial concentration of the dye, C_e is the concentration of the dye at equilibrium in mg L^{-1}, V is the volume of MO solution in liter (L) and W is the mass of PANI powder or immobilized PANI in grams (g).

The statistical analysis, coefficient of determination (R^2) and Chi-square (χ^2) test were applied to the experimental data to determine the best fitted criteria of the adsorption kinetic model. The equations are defined as the following:

$$R^2 = 1 - \frac{\Sigma_{n=1}^{n}(q_{e,\,exp.n} - q_{e,\,cal.n})^2}{\Sigma_{n=1}^{n}(q_{e,\,exp.n} - \overline{q_{e,\,exp.n}})^2} \quad (3)$$

$$\chi^2 = \Sigma_{n=1}^{n}\frac{(q_{e,\,exp.n} - q_{e,\,cal.n})^2}{q_{e,\,exp.n}} \quad (4)$$

where, $q_{e,cal}$ (mg g^{-1}) is the amount of dye adsorbed at equilibrium calculated from the model and $q_{e,exp}$ (mg g^{-1}) is the experimental values of the amount of dye adsorbed at equilibrium.

RESULTS AND DISCUSSION

1. Physical Characterization

1-1. Surface Morphology and Elemental Composition

Fig. 2 shows the SEM images of PANI powder under low (5,000x) and high magnification (30,000x). As seen in Fig. 2(a), the synthesized PANI powder particles exhibit irregular granular shape and flakes with sharp edges, while the immobilized PANI is observed to be made up of stacks of plasticized PANI aggregates as seen in Fig. 2(c). The mixing of ENR-PVC adhesive and PANI powder induced a plasticizer effect, as seen in Fig. 2(d), whereby the particles of the immobilized PANI were observed to be smaller than the PANI powder in Fig. 2(b). The percentage of the elements in PANI powder and immobilized PANI as detected by EDX is presented in Table 1. The chemical structure of PANI essentially should be made up of only carbon (C), nitrogen (N) and hydrogen (H). However, the presence of sulfur (S) and oxygen (O) elements was detected due to the addition of ammonium persulfate ($N_2H_8O_2S_2$) during the synthesis. The percentage of C increased in the PANI

Table 1. Percentage of elements presents in PANI powder and immobilized PANI

Elements	PANI powder (%)	Immobilized PANI (%)
C	67.63	70.83
N	12.10	9.15
O	16.26	15.19
S	4.01	3.00
Cl	-	1.83
Total	100.00	100.00

Table 2. BET results for PANI powder and immobilized PANI

Samples	S_{BET} ($m^2\ g^{-1}$)	Pore volume ($cm^3\ g^{-1}$)	Average pore diameter (nm)
PANI powder	9.18	0.362	15.8
Immobilized PANI	8.50	0.312	14.7

composite was due to additional C content within ENR and PVC, while other elements (N, S and O) slightly declined. Meanwhile, Cl element was detected due to the presence of chloride ions from PVC.

1-2. Surface Area and Porosity

The effect of adding ENR-PVC blend as the adhesive in the PANI formulation was analyzed via BET results in Table 2, while the corresponding isotherms of PANI powder and immobilized PANI are shown in Fig. 3. It can be observed that the presence of ENR-PVC blend in the PANI composite reduced the corresponding BET surface area, S_{BET}, average pore volume and pore diameter. The S_{BET} of the synthesized PANI powder declined from 9.18 $m^2\ g^{-1}$ to 8.50 $m^2\ g^{-1}$ meaning that the ENR-PVC blend aggregated and covered up the PANI surface. Meanwhile, the pore volume decreased from

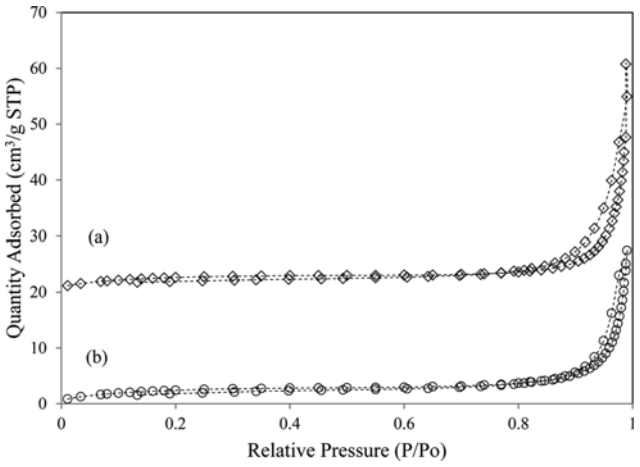

Fig. 3. Nitrogen adsorption and desorption isotherms of (a) PANI powder and (b) immobilized PANI.

0.362 to 0.312 $cm^3\ g^{-1}$ while the average pore diameter reduced from 15.8 to 14.7 nm. According to Nawi et al. [16], the reduction in the surface area and pore volume reflects low porosity and increment in the adsorbent density of the system, respectively, while the average pore diameter decreased due to the coverage of ENR-PVC adhesive on the PANI surface. The pore diameter of the synthesized PANI powder before and after the ENR-PVC addition consists of mesopores (2-50 nm) according to IUPAC classification. The isotherms of both samples in Fig. 3 show isotherm Type IV, which is associated with capillary condensation taking place in mesopores and the limiting uptake over a range of high P/P_o [44].

1-3. Fourier Transform Infrared (FTIR) Spectroscopy

Fig. 4 shows the FTIR spectra of synthesized PANI powder and immobilized PANI in the 4,000-400 cm^{-1} range. For PANI powder, the broad peak at around 3,428 cm^{-1} is contributed from N-H

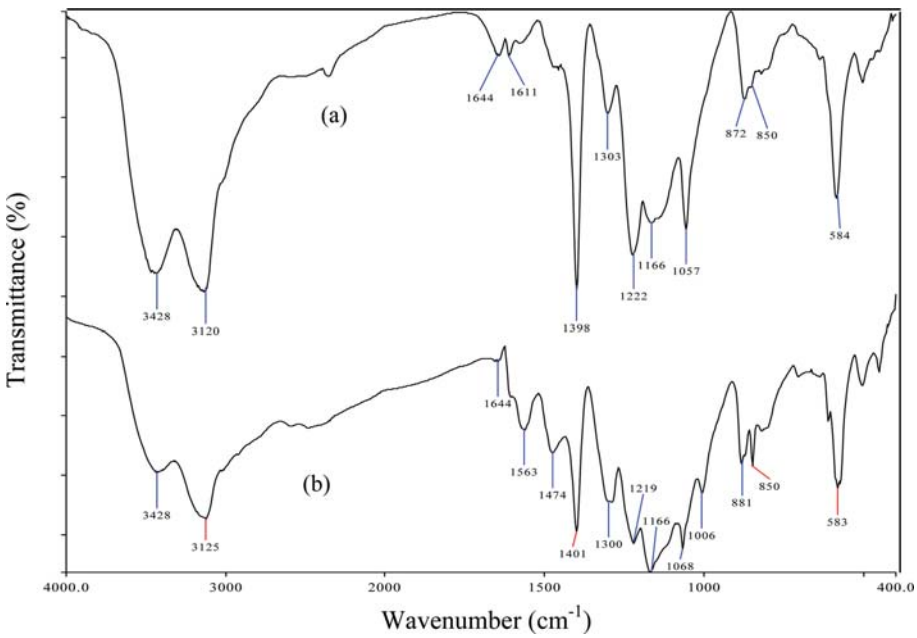

Fig. 4. FTIR spectra of (a) PANI powder and (b) immobilized PANI.

stretching vibration. The stretching of C=C in the quinoid ring and C-C stretching in benzenoid ring appear at 1,644 and 1,611 cm^{-1}, respectively [45]. Meanwhile, C-N stretching band of aromatic amine is observed at 1,474 cm^{-1}, the peak at 1,222 cm^{-1} is for C-N stretching for the benzenoid unit, and a strong band at 1,166 cm^{-1} is assigned to the electronic vibration of N quinine [46]. The peak at 872 cm^{-1} is observed due to C-H stretching for benzenoid unit [11].

For the immobilized PANI in Fig. 4(b), all the typical peaks of PANI are observed as of within the PANI powder spectrum, but the peaks are either shifted to a longer wavenumber or become less intense. However, a new peak at 1,401 cm^{-1} appears due to the overlapping peaks of C-H bending vibrations of ENR and PVC polymers within the formulation. Meanwhile, the presence of PVC, which corresponds to the C-H stretching and vibrations of the -CHCl groups in the formulation, is assigned by the peak at 1,219 cm^{-1} [40]. The peak at 1,068 cm^{-1} is due to C-O groups of ENR, while the intense peak that appears at 1,166 cm^{-1} is due to the formation of aliphatic ether, suggesting a cross-linking interaction between the two adhesive polymers [12].

1-4. UV-visible Diffuse Reflectance Spectroscopy

The UV-vis DRS spectra of the synthesized PANI powder and immobilized PANI within the wavelength range of 350 to 800 nm are shown in Fig. 5. Both types of PANI material show a similar absorption pattern throughout the wavelength range. According to Fredrick [47], the intense peak at 386 nm corresponds to the π-π^* electronic transition in the benzenoid structure involving electrons from the highest occupied molecular orbital (HOMO) to the lowest unoccupied molecular orbital (LUMO). The shoulder peak at 537 nm in both types of PANI describes the benzenoid to quinoid ring excitonic transition of the n-π^* of quinine-imine groups. Meanwhile, the absorption band in the visible region around 800 nm is assigned as the polaron band, whereby polarons are the cation radicals with unpaired electron spins and are linked to the conductivity of PANI. The broad peak around 700-800 nm for both types of PANI indicates that they were in a doped state [11].

1-5. X-ray Diffraction (XRD)

Fig. 6 shows the XRD pattern of synthesized PANI powder and immobilized PANI. A typical broad peak of amorphous scattering

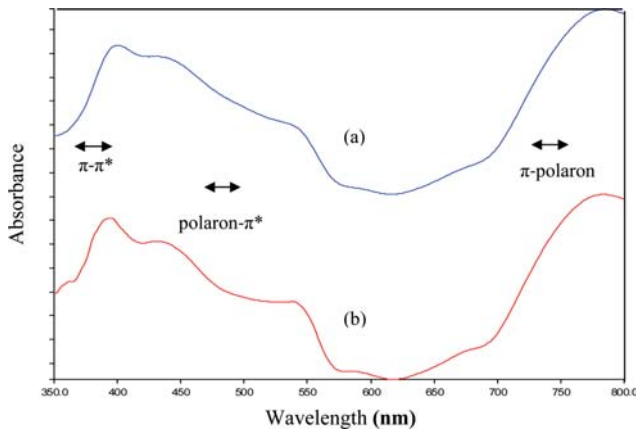

Fig. 5. UV-vis DRS spectra of; (a) PANI powder and (b) immobilized PANI.

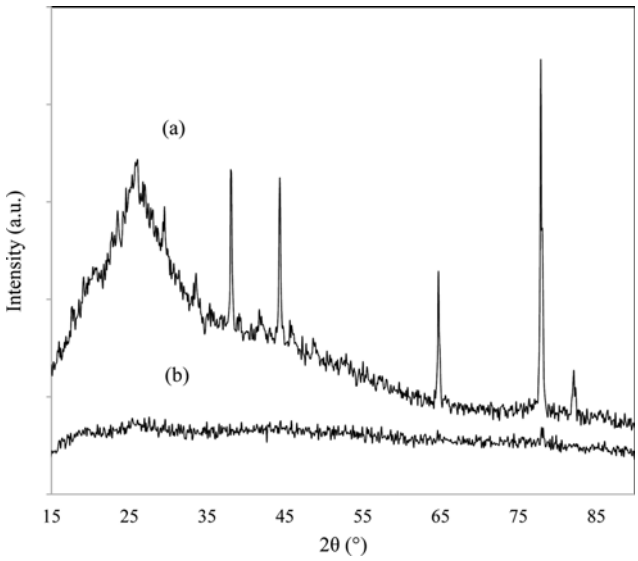

Fig. 6. XRD diffraction pattern for (a) PANI powder and (b) immobilized PANI.

of pure PANI powder was observed at around 2θ=26° [48]. On the other hand, the XRD peak of pure ENR should be at 18° [49], while the diffraction peaks of PVC appeared at 17.4° and 25.1° [50]. The corresponding peak of PANI almost disappears in the immobilized PANI pattern due to the coverage of ENR-PVC polymer, which caused the change in the crystallinity of pure PANI. This parallel XRD pattern was also observed by a carbon nanotube/PANI/PVC composite [50].

2. Effect of Operational Parameters

2-1. Effect of Aeration Flow Rate

In this study, the aeration as supplied from the aquarium air pump took over the function of stirring in the conventional adsorption set-up. The first reason is to provide a better way of providing the mass transport of dye to the vertically placed immobilized PANI. The second reason is aeration was more favorable than the stirring mode in achieving higher removal of adsorbate

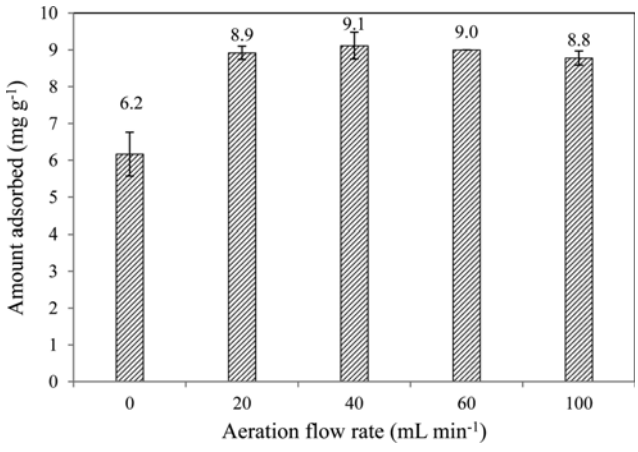

Fig. 7. The amount of MO adsorbed onto immobilized PANI under different given aeration flow rate (PANI loading=0.63 mg cm^{-2}; $[MO]_o$=20 mg L^{-1}; pH=6.5; t=90 min and T=30 °C).

as proven by Jia et al. [51] in the adsorption study of atrazine on powdered activated carbon. Thus, the aeration flow rate was controlled within the range of 0 to 100 mL min^{-1}.

As shown in Fig. 7, the immobilized PANI could still adsorb MO without any aeration with corresponding q_e of 6.2 mg g^{-1} due to the existing electrostatic attraction and concentration gradient in nature between the vacant adsorption sites of PANI and MO molecules in the bulk solution. However, a slight increment in the q_e values was observed from 8.9 to 9.1 mg g^{-1} when the aeration flow rate was increased from 20 to 40 mL min^{-1}. Within this region, the maximum contact of immobilized PANI and MO molecules was achieved as indicated by the increased q_e values. The aeration increased the intimate contact between the solid PANI and MO liquid solution as the bubbles produced certain turbulence and enhanced the mass transfer of MO molecules [51]. Eventually, the adsorption process became faster and the time to reach the adsorption equilibrium was reduced [52]. However, when the aeration rate was increased up to 100 mL min^{-1}, the q_e value started to decline slightly to 8.8 mg g^{-1} as the excessive and vigorous bubbles created a boundary layer, which reduced the contact between the MO molecules and immobilized PANI. Hence, 40 mL min^{-1} of flow rate was selected as the optimum aeration rate and was used throughout the whole experiment.

2-2. Effect of Initial pH Solution

The adsorption activity of immobilized PANI is highly dependent on the pH of the solution. For this experiment, the initial pH of MO solution in a range of 3-11 was adjusted using either HCl or NaOH where the corresponding results are shown in Fig. 8. It

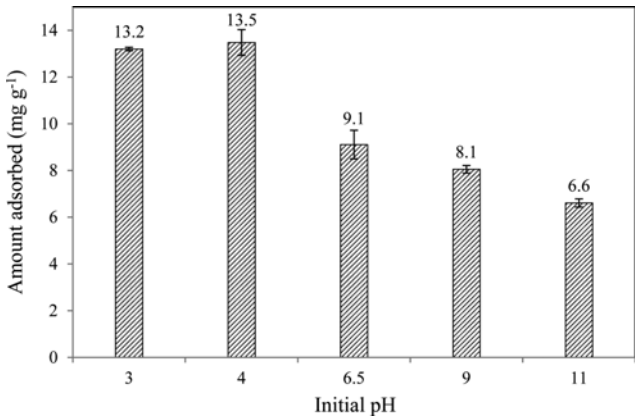

Fig. 8. The amount of MO adsorbed onto immobilized PANI at different initial pH of MO solution (PANI loading=0.63 mg cm^{-2}; $[MO]_o$=20 mg L^{-1}; aeration flow rate=40 mL min^{-1}; t=90 min and T=30 °C).

can be seen that the amount of MO adsorbed was enhanced from 13.2 to 13.5 mg g^{-1} at the corresponding pH 3 to 4, after 90 min of adsorption. However, the q_e decreased to 11.8 mg g^{-1} at ambient pH (6.5) and decreased further to 6.6 mg g^{-1} as the initial pH was increased to pH 11. Two factors have to be considered in explaining the adsorption result. Firstly, the property of the adsorbent surface charge which is highly dependent on the point of zero charge (pH_{pzc}) and secondly, the adsorbate charges in the pH-adjusted solution. The interaction between MO and immobilized PANI can be

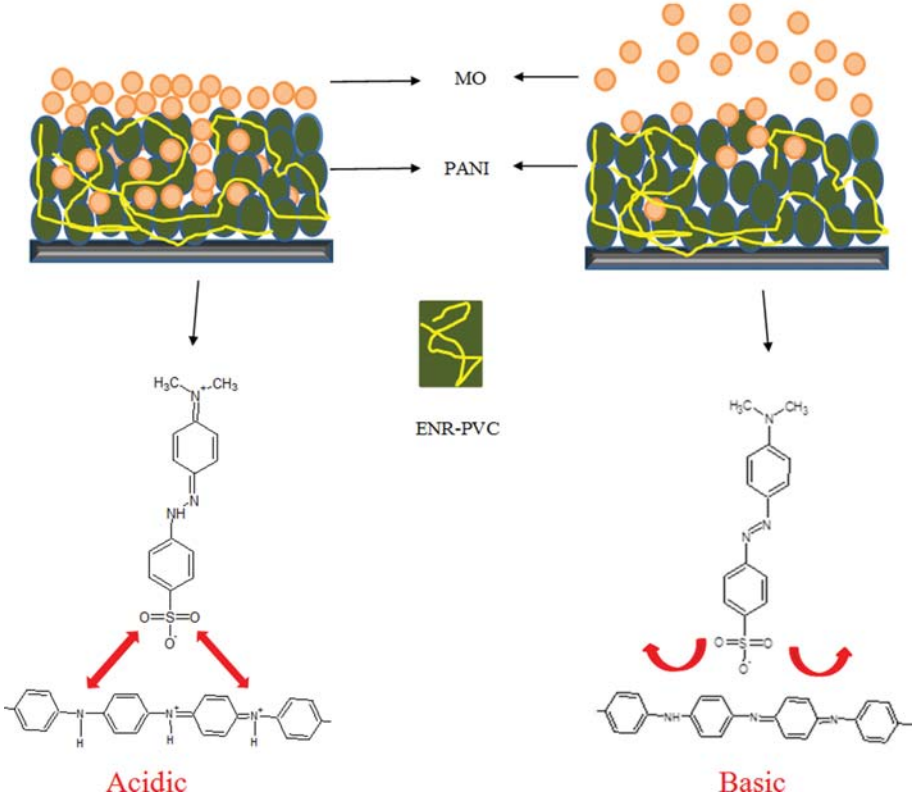

Fig. 9. The proposed mechanism of interaction between MO and immobilized PANI at different pH solution.

well understood by referring to Fig. 9. As shown in Supplementary Fig. 2, the immobilized PANI has a pH_{pzc} of 5.0. Therefore, at pH_{pzc}<5.0, the surface of immobilized PANI is positively charged while at pH_{pzc}>5.0, the surface is negatively charged. In this case, any negatively charged dyes can be attracted to the immobilized PANI under pH<5, while it is the opposite for the positively charged dyes which adsorb over pH 5. The second factor is the effect of the dye acid dissociation constant (pKa) on the adsorption. It is known that the pKa of MO solution is 3.8 [48]. Below pH 3.8, the amine functional group of MO will be protonated. A slight reduction in the amount of MO adsorbed at pH 3 was observed due to the repulsion of the protonated amine groups in MO and the positively charged PANI, which existed in emeraldine salt form (ES) [48].

When the pH of the MO solution is greater than 3.8, the sulfonate functional group of MO ($-SO_3Na$) dissociates and produces anionic species that are negatively charged ($-SO_3$). At pH 4, the electrostatic attraction between the positively charged amino groups of PANI and the negatively charged sulfonate groups of MO is significant, which explains the higher amount of MO adsorbed onto the immobilized PANI in that region. At higher pH than pH_{pzc} (pH 5), the amount of MO adsorbed onto PANI declined, especially in a very basic pH solution, since the negatively charged sulfonate groups of MO dye experienced electrostatic repulsion by the negative backbone of PANI. Another functional group of MO, the amine group would be unchanged under neutral and alkaline condition [48]. The presence of more HO^- ions in MO solution in this pH region further inhibited the adsorption occurrence. Nevertheless, the ambient pH was chosen as the working pH to avoid changes in molecular structure (color change) of MO.

3. Adsorption Studies

3-1. Adsorption Kinetic

A kinetic study of immobilized PANI was conducted at dye concentrations of 20-60 mg L^{-1} and was compared against PANI powder in the suspended mode. The collected data were fitted into the Lagergren's pseudo-first (Eq. (5)), Ho and Mc Kay's pseudo-second (Eq. (6)) [53] and Weber and Morris's intra-particle diffusion (Eq. (7)) [54] kinetic models that were shown below. A good coefficient of determination (R^2) and small Chi-square (χ^2) value between the experimental data and calculated data explain the actual adsorption mechanism of the system.

$$\log(q_e - q_t) = \log q_e - \left(\frac{k_1}{2.303}\right)t \quad (5)$$

where, q_e and q_t are the sorption capacity at equilibrium and at time (t), respectively (mg g^{-1}) and k_1 is the rate constant of pseudo-first order sorption (min^{-1}). A straight plot of log ($q_e - q_t$) against time (t) will give k_1 and q_e from the slope and intercept, respectively.

$$\frac{t}{q_t} = \frac{1}{k^2 q_e^2} + \left(\frac{1}{q_e}\right)t \quad (6)$$

where, k_2 is the rate constant of pseudo-second order (g $mg^{-1}min^{-1}$). A straight plot of log t/q_t against time (t) will give k_2 and q_e from the slope and intercept, respectively.

$$q_t = k_{id} t^{1/2} + C \quad (7)$$

where, k_d (mg g^{-1} $min^{-1/2}$) is the intra-particle diffusion rate constant and is calculated by plotting q_t versus $t^{1/2}$, i is the adsorption stage while C is the y-intercept corresponding to the degree of boundary layer thickness.

As shown in Table 3, the adsorption of MO onto the immobilized and suspended PANI system is best described by the pseudo-second-order model since all R^2 values at different MO concentrations exceed 0.99. Furthermore, the $q_{e,cal}$ of all concentrations and systems were closely agreeable with $q_{e,exp}$ as indicated by the smaller Chi-square values. The pseudo-second-order rate constants (k_2)

Table 3. Kinetic parameters for the adsorption of MO onto immobilized and suspended PANI (PANI loading=0.63 mg cm^{-2} or 20 mg by weight; aeration flow rate=40 mL min^{-1}; pH=6.5; t=90 min and T=30 °C)

Model	Parameters	Immobilized				Suspended			
	C_o (mg g^{-1})	20	30	40	60	20	30	40	60
Pseudo-first-order	$q_{e,exp}$ (mg g^{-1})	16.6	26.8	36.0	46.8	16.3	26.3	36.1	46.4
	$q_{e,cal}$ (mg g^{-1})	14.6	21.9	27.9	38.8	10.1	17.5	24.7	33.3
	k_1 (min^{-1})	0.020	0.022	0.029	0.022	0.082	0.074	0.066	0.046
	R^2	0.892	0.882	0.863	0.770	0.866	0.883	0.882	0.755
	χ^2	5.34	7.07	3.64	10.4	2.39	2.94	3.62	3.69
Pseudo-second-order	$q_{e,cal}$ (mg g^{-1})	9.60	16.7	25.5	27.0	13.0	27.9	38.2	48.5
	$k_2 \times 10^{-3}$ (g $mg^{-1}min^{-1}$)	7.01	8.20	1.95	0.08	0.36	0.21	0.08	0.03
	R^2	0.995	0.995	0.995	0.995	1.00	1.00	0.997	0.999
	χ^2	0.418	1.16	1.47	2.60	0.69	0.11	0.12	1.85
Intra-particle diffusion	$k_{id\ 1}$ (mg g^{-1} $min^{-1/2}$)	1.67	3.05	4.74	5.80	3.86	5.91	7.74	9.47
	R^2	0.985	0.993	0.969	0.992	0.916	0.915	0.883	0.796
	C	-	-	-	-	2.34	3.69	5.82	9.87
	$k_{id,2}$ (mg g^{-1} $min^{-1/2}$)	0.932	1.34	1.45	2.47	0.285	0.559	1.13	2.58
	R^2	0.995	0.992	0.999	0.968	0.762	0.714	0.873	0.976
	$k_{id,3}$ (mg g^{-1} $min^{-1/2}$)	0.533	0.858	1.13	1.79	0.051	0.140	0.446	0.960
	R^2	0.987	0.994	0.998	0.998	1.00	1.00	1.00	1.00

decreased as the initial concentration increased for both immobilized and suspended PANI. The k_2 values reduced from 7.01 to 0.01×10^{-3} g mg^{-1}min^{-1} and 0.36 to 0.03×10^{-3} g mg^{-1}min^{-1} for immobilized and suspended PANI, respectively. Comparatively, immobilized PANI has higher k_2 values than suspended PANI for all the concentrations, which means that PANI powder in immobilized form has a higher affinity for MO adsorption than in powdered form. However, the amount of MO adsorbed was less than its counterpart suspended mode due to fewer adsorption sites of PANI in immobilized form.

As Ho and Mc Kay's pseudo-second-order kinetic model can only explain the process on the surface of PANI, the adsorption data were then plotted according to Weber and Morris's intra-particle diffusion kinetic model (Eq. (7)). According to this model, the intra-particle diffusion controlled solely the adsorption process if the plot crossed the origin. Both figures show multilinear portions, suggesting that there is more than one process for the adsorption process [55]. For immobilized PANI in Fig. 10(a), the linear plot for all concentrations crossed the origin at stage 1, which obeys the Weber and Morris statement that the intra-particle diffusion is the predominant mechanism throughout the adsorption process. Minimal and negligible effect of external film control was observed at this stage. At the second stage, low diffusion rates were observed, indicating slow diffusion of MO from the adsorbent surface to the intra-particle active sites within the PANI layer [56].

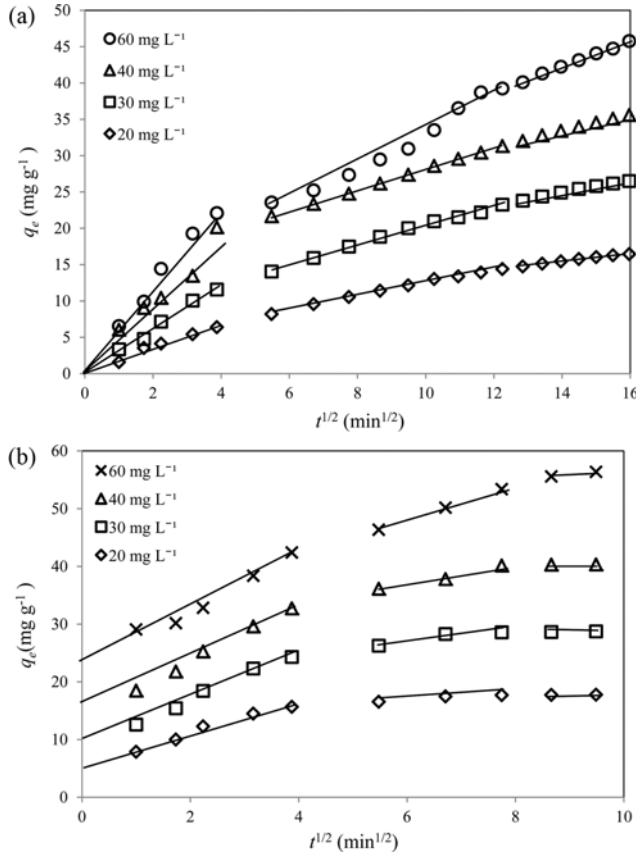

Fig. 10. Intraparticle diffusion plots for the adsorption of MO onto; (a) immobilized PANI and (b) suspended PANI.

The diffusion resistance increased; thus, the rate decreased during this stage. As the remaining MO in bulk solution was reduced, the diffusion process rate became slower and reached final equilibrium, denoted as the third stage [17]. According to Ngoh and Nawi [17], when the system is immobilized on a flat surface support material, intra-particle diffusion will dominate the rate-controlling step. They added that the effective adsorption process depends on the mobility or diffusion of the dye molecules from the outer surface of the adsorbent through the inner layers until no more diffusion can occur due to the low concentration of the remaining solution.

For suspended PANI in Fig. 10(b), stage 1 started from 1-15 min, stage 2 from 30-60 min and stage 3 from 75-90 min of adsorption. Stage 1 did not cross the origin, so there was no intra-particle diffusion involved in the adsorption process. The order of adsorption rate is $k_{id1}>k_{id2}>k_{id3}$ for the three stages, while the rates for each stage became faster with increased concentrations. The C values also increased with the increasing concentrations, which corresponded to thicker boundary layer or external mass transfer resistance for the adsorption of MO onto the suspended PANI. Hence, the adsorption of MO via suspended mode was controlled predominantly by film diffusion. At stage 1, the fastest rate was due to rapid adsorption of MO onto the abundant adsorption sites of PANI powder with minimal or negligible external mass transfer resistance. The rates became slower at stage 2 as the diffusion by the internal layers of PANI powder reached saturation. At the third stage, the diffusion was the slowest as the MO concentration in the solution decreased and the system reached equilibrium.

3-2. Adsorption Isotherm

Langmuir isotherm (Eq. (8)) assumes that the adsorption is monolayer coverage, homogeneous, and all adsorption sites are equal [57].

$$\frac{C_e}{q_e}=\frac{C_e}{q_m}+\frac{1}{q_m b_L} \tag{8}$$

where, q_m is the maximum amount of MO adsorbed (mg g^{-1}) and b_L is the Langmuir constant (L mg^{-1}). The values of q_m and b_L were obtained from the slope and intercept of the plot of $1/q_e$ versus $1/C_e$.

Freundlich isotherm (Eq. (9)), on the other hand, is applicable to a heterogeneous multilayer surface, has different adsorption affinity which is suitable for middle and high concentrations of solutes but not for low concentration [58].

$$\log q_e=\log K_F+\frac{1}{n_F}\log C_e \tag{9}$$

where K_F is the Freundlich constant (L g^{-1}) and n_F is the adsorption intensity. A plot of log q_e and log C_e would give linearity with the slope and intercept given as n_F and K_F, respectively.

Dubinin-Radushkevich (D-R) isotherm (Eq. (10)) can be used to distinguish whether physisorption or chemisorption governs the adsorption process [57].

$$\ln q_e=\ln q_d-\beta\varepsilon^2,\quad \varepsilon=RT\ln\left(1+\frac{1}{C_e}\right). \tag{10}$$

where q_d is the maximum capacity (mg g^{-1}), ε is the Polanyi poten-

tial, R is the universal gas constant (8.314 J $mol^{-1}K^{-1}$), T is the absolute temperature (K) and E is the mean adsorption energy as derived from $E=1/\sqrt{2\beta}$. The plot of log q_e versus ε^2 would provide the β and q_d from the slope and intercept, respectively.

Temkin isotherm (Eq. (11)) assumes that the heat of adsorption of all the molecules in the layer decreases linearly with coverage due to the adsorbent-adsorbate interactions, and that the adsorption is characterized by a uniform distribution of binding energies, up to some maximum binding energy [57].

$$q_e = \frac{RT}{b_T}\ln K_T + \frac{RT}{b_T}\ln C_e \quad (11)$$

where K_T is the Temkin isotherm equilibrium binding constant (L g^{-1}) and b_T is the Temkin isotherm constant. The plot of q_e versus ln C_e would give K_T and b_T as the slope and intercept, respectively.

Fig. 11(a)-(d) shows the plotted data based on the isotherm models, while Table 4 tabulates their parameter constants. The immobilized and suspended PANI systems obeyed the Freundlich isotherm than the other models based on the best value of the coefficient of determination, R^2 with 0.927 and 0.999, respectively. According to this model, the adsorption sites in both systems are heterogeneous, multilayer and have a different affinity. The value of n_F represents the favorability of the system: one is unity, more than one means the adsorption is favorable at high concentrations, and less than one indicates the unfavorability of the system [10]. In addition, n_F can also be represented as $1/n_F$ which shows the degree of surface heterogeneity [58]. The n_F value and the calculated $1/n_F$ were 1.89 and 0.53 for immobilized PANI, while they were 1.26 and 0.79 for suspended PANI, respectively, which means that the adsorption sites in the immobilized and suspended PANI were favorable at high concentration and showed heterogeneity. This also shows that the presence of ENR-PVC adhesive did not affect the characteristics of the adsorption sites within the PANI composite.

Table 4. Isotherm parameter constants for the adsorption of MO onto immobilized and suspended PANI (PANI loading= 0.63 mg cm^{-2} or 20 mg by weight; aeration flow rate=40 mL min^{-1}; pH=6.5; t=90 min and T=30 °C)

Isotherm models	Parameters	Immobilized	Suspended
Langmuir	b_L (L mg^{-1})	0.01	0.06
	q_m (mg g^{-1})	77.5	125
	R^2	0.838	0.950
Freundlich	n_F	1.89	1.26
	K_F (L g^{-1})	12.4	8.15
	R^2	0.927	0.999
Dubinin Radushkevich	q_d (mg g^{-1})	47.3	35.1
	β (kJ mol^{-1})	0.71	0.91
	R^2	0.860	0.853
Temkin	K_T (L g^{-1})	1.00	1.00
	b_T (KJ mol^{-1})	22.1	23.0
	R^2	0.860	0.940

Supplementary Table 1 lists the comparison of maximum adsorp-

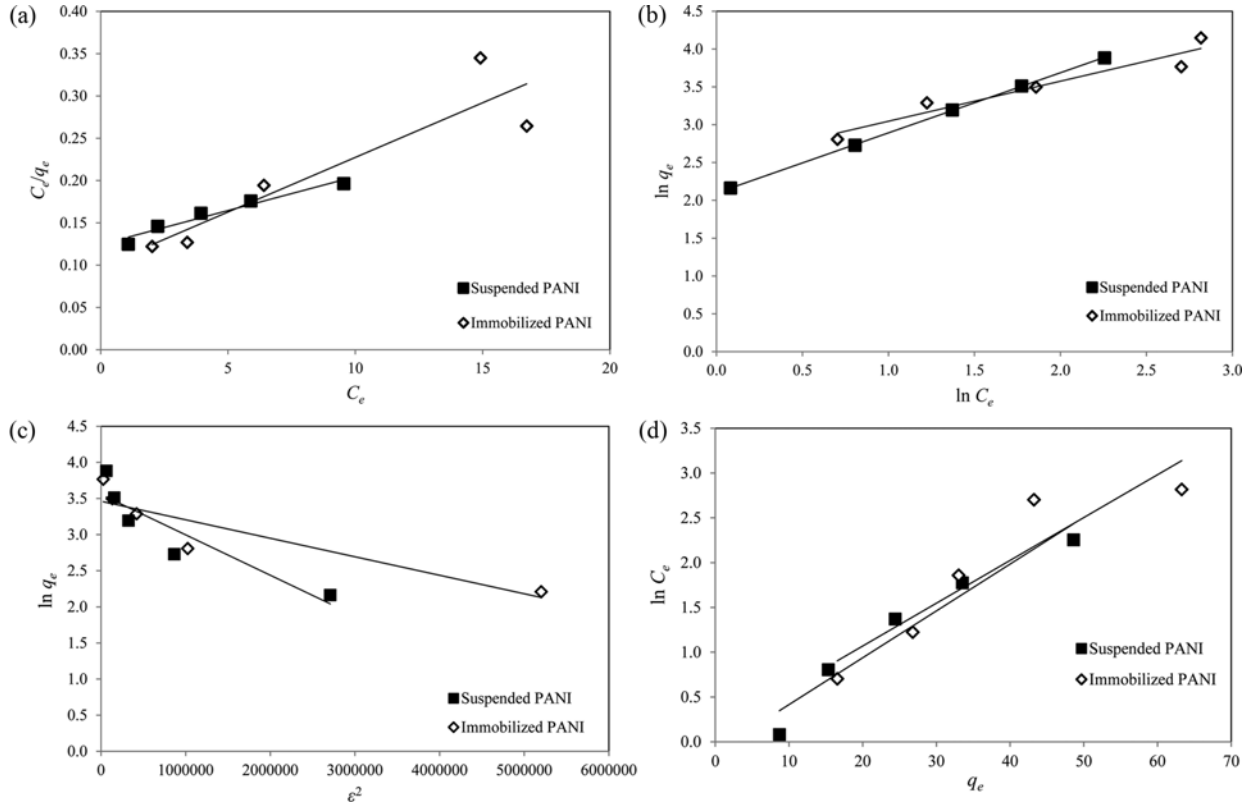

Fig. 11. Isotherm plot for the adsorption of MO onto immobilized and suspended PANI based on (a) Langmuir, (b) Freundlich, (c) Dubinin-Radushkevich and (d) Temkin model.

tion capacities (q_m) of PANI-based adsorbents for the adsorption of MO. It can be seen that the q_m of PANI powder produced in this study was 125 mg g^{-1} and was comparable with other adsorbents such as PANI-attapulgite and PANI-cobalt oxide. This is important since the powdered adsorbent utilized for immobilization which needed to have high q_m as its BET surface area was expected to be reduced after immobilization [15]. Interestingly, the q_m of the immobilized PANI in this study was still better than the magnetic PANI and PANI/polyamide 6 adsorbents in the suspended mode, which shows that PANI in the immobilized form is possible to be used in the dye waste treatment.

3-3. Adsorption Thermodynamic

Adsorption studies at different temperatures are essential to see the relationship between the given heat towards the adsorption characteristics of an adsorbent and its adsorbates. The adsorption study was done in a water bath adjusted to the desired temperature of 30-60 °C. The thermodynamic variables such as the changes in Gibbs free energy (ΔG^o), enthalpy (ΔH^o) and entropy (ΔS^o) are determined from the following equations [16]:

$$K_C = \frac{C_{Ae}}{C_e} \tag{12}$$

$$\Delta G^o = -RT\log K_C \tag{13}$$

$$\log K_C = \frac{\Delta S^o}{2.303R} - \frac{\Delta H^o}{2.303RT} \tag{14}$$

where, K_C is the equilibrium constant, C_{Ae} is the concentration of MO adsorbed on PANI solid at equilibrium (mg L^{-1}), C_e is the concentration of MO in the liquid phase (mg L^{-1}) at equilibrium, T is the absolute temperature (K) and R is the universal gas constant (8.314 J $mol^{-1}K^{-1}$). The values of ΔH^o and ΔS^o were calculated from the slope and intercept of the van't Hoff plot of log K_C versus 1/T, respectively.

The negative and increasing in ΔG^o values with temperature in Table 5 show that the adsorption process of MO onto the immobilized PANI was spontaneous but became increasingly unfavorable at high temperature. Meanwhile, the negative value of ΔH^o and smaller K_C and q_e suggest that the adsorption process was exothermic and MO would rather be in the bulk solution than being adsorbed onto immobilized PANI at high temperatures. In addition, the negative value of ΔS^o value indicates the decrease in the randomness and affinity of a solid/liquid interface during the adsorption of MO onto the immobilized PANI at elevated temperatures. For suspended PANI, the decreasing ΔG^o values with temperature explains that the adsorption process became increasingly spontaneous as more MO was adsorbed onto suspended PANI. The positive values for ΔH^o and ΔS^o in the case of suspended PANI were related to the endothermicity of adsorption MO at high temperature. This phenomenon increased the randomness of MO and suspended PANI as the water molecules were being replaced by the dye molecules during the adsorption process [20]. Nevertheless, the thermodynamic study of MO onto suspended PANI was in line with the reported works on methylene blue [20], reactive black 5 [59] and Congo red [60].

Table 5. Thermodynamic parameters for the adsorption of MO onto immobilized and suspended PANI (PANI loading=0.63 mg cm^{-2} or 20 mg by weight; $[MO]_o$=20 mg L^{-1}; aeration flow rate=40 mL min^{-1}; pH=6.5; t=90 min and T=30 °C)

Temperature (K)	Immobilized				
	K_C	q_e (mg g^{-1})	ΔG^o (kJ mol^{-1})	ΔH^o (kJ mol^{-1})	ΔS^o (J mol^{-1} K^{-1})
303	1.26	9.10	−2.74	−29.7	−96.0
318	1.08	5.51	−2.08		
333	0.37	4.41	−0.59		
Temperature (K)	Suspended				
	K_C	q_e (mg g^{-1})	ΔG^o (kJ mol^{-1})	ΔH^o (kJ mol^{-1})	ΔS^o (J mol^{-1} K^{-1})
303	3.81	14.2	−3.70	37.6	135.8
318	7.08	15.8	−5.18		
333	17.3	17.1	−7.19		

4. Reusability of Immobilized PANI

The conventional suspended system suffers from the need of filtration after treatment, which is tedious, costly and time-consuming. With the immobilized system, all those works can be avoided. The reusability and efficiency of immobilized PANI were evaluated for three cycles in terms of percentage removal as seen in Fig. 12. During the first, second and third cycles, the percentage of removal was 97.6%, 95.9% and 93.4%, respectively. The reduced uptake by the immobilized adsorbent for the second and third cycles was due to fewer accessible adsorption sites for a new fresh solution of MO. In addition, the process of cleaning the surface of immobilized PANI with water between each cycle could not effectively desorb the adsorbed MO on the PANI surface. However, as proven, a high removal efficiency of MO can still be achieved for the three cycles, showing that the immobilized PANI is recyclable and highly effective for real scale applications.

CONCLUSION

Immobilized PANI powder was successfully fabricated on glass

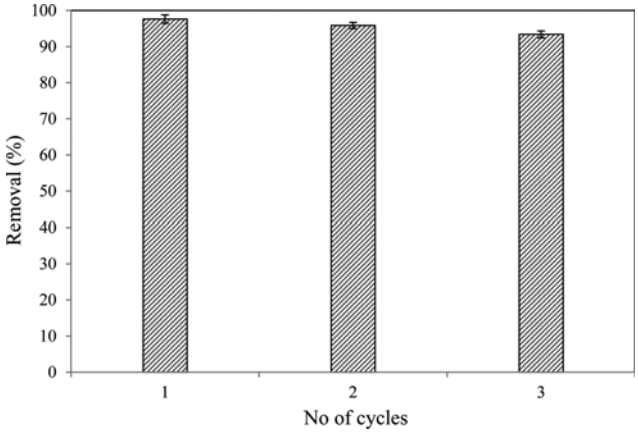

Fig. 12. The removal efficiency of immobilized PANI for the adsorption of 20 mg L^{-1} MO for three cycles of application (PANI loading=0.63 mg cm^{-2}; $[MO]_o$=20 mg L^{-1}; aeration flow rate=40 mL min^{-1}; pH=6.5; t=90 min and T=30 °C).

plates for the removal of MO dye. The immobilization of PANI powder produced plasticized PANI aggregates which reduced its S_{BET}, pore volume and pore diameter. The adsorption kinetic and isotherm studies showed that the adsorption of MO onto immobilized and suspended mode of PANI obeyed the pseudo-second-order and Freundlich model. These implied that the adsorption sites of immobilized PANI were heterogeneous and the adsorption occurred in multilayer state. Meanwhile, the intra-particle diffusion was the rate-controlling step for immobilized PANI, while the external film resistance controlled the adsorption in suspended mode. The thermodynamic study of immobilized PANI also elucidated that the adsorption process could reduce the operation cost as it works better at room temperature, which was in contrast to the suspended PANI. The immobilization of PANI powder eliminates the need for filtration of post-treatment and proves that immobilized PANI can become another potential adsorbent that has high capacity, recyclability and removal efficiency for wastewater treatment.

ACKNOWLEDGEMENTS

The authors would like to thank Universiti Sains Malaysia for the research facilities and financial support through FRGS grant (203/PKIMIA/6711228). N.N. Bahrudin is grateful to the Malaysian Ministry of Higher Education for the scholarship under My Brain 15 programme.

SUPPORTING INFORMATION

Additional information as noted in the text. This information is available via the Internet at http://www.springer.com/chemistry/journal/11814.

REFERENCES

1. I. Ali, Z. A. Al-Othman and A. Alwarthan, *J. Mol. Liq.*, **224**, 171 (2016).
2. S. Sharma and A. Imran, *J. Toxicol. Environ. Health*, **3**, 286 (2011).
3. Z. Sareban and V. Javanbakht, *Korean J. Chem. Eng.*, **34**, 2886 (2017).
4. I. Ali, Z. A. Al-Othman and A. Al-Warthan, *Desalin. Water Treat.*, **57**, 10409 (2016).
5. I. Ali, Z. Al-Othman and A. Al-Warthan, *Int. J. Environ. Sci. Technol.*, **13**, 733 (2016).
6. I. Ali, Z. A. Al-Othman and A. Alwarthan, *J. Mol. Liq.*, **219**, 858 (2016).
7. I. Ali, Z. A. Al-Othman and O. M. Alharbi, *J. Mol. Liq.*, **218**, 465 (2016).
8. M. Tanzifi, M. T. Yaraki, A. D. Kiadehi, S. H. Hosseini, M. Olazar, A. K. Bhati, S. Agarwal, V. K. Gupta and A. Kazemi, *J. Colloid Interface Sci.*, **510**, 246 (2018).
9. I. Ali, T. A. Khan and M. Asim, *Environ. Sci. Pollut. Res.*, **19**, 1668 (2012).
10. S. Duan, X. Xu, X. Liu, Y. Wang, T. Hayat, A. Alsaedi, Y. Meng and J. Li, *J. Colloid Interface Sci.*, **513**, 92 (2018).
11. S. Razak, M. A. Nawi and K. Haitham, *Appl. Surf. Sci.*, **319**, 90 (2014).
12. M. A. Nawi, Y. S. Ngoh and S. M. Zain, *Int. J. Photoenergy*, **2012**, 12 (2012).
13. R. Bochenek, R. Sitarz and D. Antos, *Chem. Eng. Sci.*, **66**, 6209 (2011).
14. I. Ali, Z. A. Al-Othman, A. Alwarthan, M. Asim and T. A. Khan, *Environ. Sci. Pollut. Res.*, **21**, 3218 (2014).
15. N. N. Bahrudin and M. A. Nawi, *React. Kinet. Mech. Cat.*, **124**, 153 (2018).
16. M. A. Nawi, S. Sabar, A. H. Jawad, Sheilatina and W. S. Wan Ngah, *Biochem. Eng. J.*, **49**, 317 (2010).
17. Y. S. Ngoh and M. A. Nawi, *Int. J. Environ. Sci. Technol.*, **13**, 907 (2016).
18. I. Ali, Z. A. Al-Othman and A. Alwarthan, *J. Mol. Liq.*, **221**, 1168 (2016).
19. I. Ali, Z. A. Alothman and A. Alwarthan, *J. Mol. Liq.*, **236**, 205 (2017).
20. R. Ansari, A. Mohammad-khah and M. Nazmi, *Current Chem. Lett.*, **2**, 215 (2013).
21. M. H. Dehghani, D. Sanaei, I. Ali and A. Bhatnagar, *J. Mol. Liq.*, **215**, 671 (2016).
22. J. Wang, S. Ding, C. Zheng, H. Ma and Y. Ji, *Desalin. Water Treat.*, **40**, 92 (2012).
23. T. K. Mahto, S. Chandra, C. Haldar and S. K. Sahu, *RSC Adv.*, **5**, 47909 (2015).
24. S. Zaremotlagh and A. Hezarkhani, *Environ. Earth Sci.*, **71**, 2999 (2014).
25. S. Zhang, M. Zeng, W. Xu, J. Li, J. Li, J. Xu and X. Wang, *Dalton Transactions*, **42**, 7854 (2013).
26. D. Shao, G. Hou, J. Li, T. Wen, X. Ren and X. Wang, *Chem. Eng. J.*, **255**, 604 (2014).
27. S. Palaniappan and A. John, *Prog. Polym. Sci.*, **33**, 732 (2008).
28. B. T. Deepshikha and T. Basu, *Res. J. Chem. Sci.*, **1**, 20 (2011).
29. S. Xing, C. Zhao, S. Jing and Z. Wang, *Polymer*, **47**, 2305 (2006).
30. Q. Guo, C. Yi, L. Zhu, Q. Yang and Y. Xie, *Polymer*, **46**, 3185 (2005).
31. C. H. Yang, L. R. Huang, Y. K. Chih, W. C. Lin, F. J. Liu and T. L. Wang, *Polymer*, **48**, 3237 (2007).
32. A. F. Diaz and J. A. Logan, *J. Electroanal. Chem. Interfacial. Electrochem.*, **111**, 111 (1980).
33. E. M. Genies, A. A. Syed and C. Tsintavis, *Mol. Cryst. Liq. Cryst.*, **121**, 181 (1985).
34. X. Jing, Y. Wang, D. Wu and J. Qiang, *Ultrason. Sonochem.*, **14**, 75 (2007).
35. D. K. Bandgar, G. D. Khuspe, R. C. Pawar, C. S. Lee and V. B. Patil, *Appl. Nanosci.*, **4**, 27 (2014).
36. J. Huang, S. Virji, B. H. Weiller and R. B. Kaner, *J. Am. Chem. Soc.*, **125**, 314 (2003).
37. K. Gupta, P. T. Das, T. K. Nath, A. K. Meikap and P. C. Jana, *Polym. Compos.*, **36**, 489 (2015).
38. R. E. Morsi, E. A. Khamis and A. M. Al-Sabagh, *J. Taiwan Inst. Chem. Eng.*, **60**, 573 (2016).
39. M. Bhaumik, C. Noubactep, V. K. Gupta, R. I. McCrindle and A. Maity, *Chem. Eng. J.*, **271**, 135 (2015).
40. M. A. Nawi and S. M. Zain, *Appl. Surf. Sci.*, **258**, 6148 (2012).
41. R. Othaman, Y. H. Yuan and M. A. Bakar, *Orient. J. Chem.*, **31**, 697 (2015).
42. U. Ishiaku, *Plast. Eng.*, **52**, 663 (1999).

43. C. T. Ratnam, M. Nasir, A. Baharin and K. Zaman, *Polym. Degrad. Stab.*, **72**, 147 (2001).
44. K. S. W. Sing, *Pure Appl. Chem.*, **54**, 2201 (1982).
45. S. Palaniappan and C. A. Amarnath, *React. Funct. Polym.*, **66**, 1741 (2006).
46. S. Min, F. Wang and Y. Han, *J. Mater. Sci.*, **42**, 9966 (2007).
47. O. Fredrick, M. Mangaka and M. Fatoki, O, *J. Chem. Sci.*, **1**, 29 (2013).
48. K. Haitham, S. Razak and M. A. Nawi, *Arab. J. Chem.* (2014), DOI:10.1016/j.arabjc.2014.10.010.
49. M. Soheilmoghaddam, M. Uzir Wahit and N. Ibrahim Akos, *Mater. Lett.*, **111**, 221 (2013).
50. H.-x. Tan and X.-c. Xu, *Composites Sci. Technol.*, **128**, 155 (2016).
51. Y. Jia, R. Wang, A. G. Fane and W. B. Krantz, *Sep. Purif. Technol.*, **46**, 79 (2005).
52. S. Larous, A.-H. Meniai and M. B. Lehocine, *Desalination*, **185**, 483 (2005).
53. Y. S. Ho and G. McKay, *Process Biochem.*, **34**, 451 (1999).
54. W. J. Webern and J. C. Morris, *J. Sanit. Eng. Div. Am. Soc. Civ. Eng.*, **89**, 31 (1963).
55. S. Duan, J. Li, X. Liu, Y. Wang, S. Zeng, D. Shao and T. Hayat, *ACS Sustainable Chem. Eng.*, **4**, 3368 (2016).
56. S. Duan, Y. Wang, X. Liu, D. Shao, T. Hayat, A. Alsaedi and J. Li, *ACS Sustainable Chem. Eng.*, **5**, 4073 (2017).
57. K. Y. Foo and B. H. Hameed, *Chem. Eng. J.*, **156**, 2 (2010).
58. W. S. W. Ngah and S. Fatinathan, *J. Environ. Manage.*, **91**, 958 (2010).
59. M. Bhaumik, R. I. McCrindle, A. Maity, S. Agarwal and V. K. Gupta, *J. Colloid Interface Sci.*, **466**, 442 (2016).
60. S. Debnath, N. Ballav, A. Maity and K. Pillay, *Int. J. Biol. Macromol.*, **75**, 199 (2015).
61. Y. Xia, T. Li, J. Chen and C. Cai, *Synth. Met.*, **175**, 163 (2013).
62. C. Yao, Y. Zeng, Y. Cao, W. Li and X. Zheng, *J. Chin. Ceram. Soc.*, **38**, 671 (2010).
63. S. Shahabuddin, N. M. Sarih, S. Mohamad and S. N. A. Baharin, *RSC Adv.*, **6**, 43388 (2016).